© 2014. Published by The Company of Biologists Ltd | The Journal of Experimental Biology (2014) 217, 3805-3814 doi:10.1242/jeb.106732

RESEARCH ARTICLE

Hyperactivation of L-type voltage-gated Ca^{2+} channels in *Caenorhabditis elegans* striated muscle can result from point mutations in the IS6 or the IIIS4 segment of the α1 subunit

Viviane Lainé, Jean Rony Ségor, Hong Zhan, Jean-Louis Bessereau and Maelle Jospin*

ABSTRACT

Several human diseases, including hypokalemic periodic paralysis and Timothy syndrome, are caused by mutations in voltage-gated calcium channels. The effects of these mutations are not always well understood, partially because of difficulties in expressing these channels in heterologous systems. The use of *Caenorhabditis elegans* could be an alternative approach to determine the effects of mutations on voltage-gated calcium channel function because all the main types of voltage-gated calcium channels are found in *C. elegans*, a large panel of mutations already exists and efficient genetic tools are available to engineer customized mutations in any gene. In this study, we characterize the effects of two gain-of-function mutations in *egl-19*, which encodes the L-type calcium channel α_1 subunit. One of these mutations, *ad695*, leads to the replacement of a hydrophobic residue in the IIIS4 segment. The other mutation, *n2368*, changes a conserved glycine of IS6 segment; this mutation has been identified in patients with Timothy syndrome. We show that both *egl-19* (gain-of-function) mutants have defects in locomotion and morphology that are linked to higher muscle tone. Using *in situ* electrophysiological approaches in striated muscle cells, we provide evidence that this high muscle tone is due to a shift of the voltage dependency towards negative potentials, associated with a decrease of the inactivation rate of the L-type Ca^{2+} current. Moreover, we show that the maximal conductance of the Ca^{2+} current is decreased in the strongest mutant *egl-19(n2368)*, and that this decrease is correlated with a mislocalization of the channel.

KEY WORDS: *Caenorhabditis elegans*, Ca^{2+} channel, L-type, Mutation, Muscle

INTRODUCTION

Calcium ions play multiple roles in cell physiology, starting from the initiation of a one-cell growth during fertilization to its termination by apoptosis. Among the molecules involved in fine-tuning of Ca^{2+} homeostasis, voltage-gated Ca^{2+} channels are responsible for local and transient increases of intracellular Ca^{2+} concentration. Based on pharmacological and biophysical properties, voltage-gated Ca^{2+} channels are classified into three families: the L-type, the P/Q/R/N-type and the T-type channels (Catterall, 2011). L-type channels have been shown to play crucial roles in Ca^{2+} homeostasis of excitable cells. Dysfunction of these channels has been reported in several congenital disorders, including hypokalemic periodic paralysis (hypoPP), malignant hyperthermia or Timothy syndrome (Jurkat-Rott et al., 1994; Ptácek et al., 1994; Monnier et al., 1997; Splawski et al., 2004). The molecular bases of these channelopathies have been well described: mutations are located at multiple sites of the pore-forming and voltage-sensor regions of the α_1 subunit. The α_1 subunit is composed of four equivalent domains (named I to IV) containing six transmembrane segments (named S1 to S6) and linked to each other by large cytoplasmic loops (Catterall, 2011).

In hypoPP and malignant hyperthermia, most mutations target the arginine residues in the S4 voltage-sensor segments of the skeletal subunit CACNA1S (Jurkat-Rott et al., 1994; Ptácek et al., 1994; Monnier et al., 1997; Wang et al., 2005; Chabrier et al., 2008; Carpenter et al., 2009; Ke et al., 2009; Pirone et al., 2010; Toppin et al., 2010; Hirano et al., 2011; Li et al., 2012). In Timothy syndrome, two glycine residues in IS6 segment have been reported to be mutated in the cardiac and neuronal subunit CACNA1C (Splawski et al., 2004; Splawski et al., 2005). Understanding the functional effects of these L-type channel mutations is a prerequisite to develop new therapeutic strategies. However, the physiological consequences of the mutations are still poorly understood. Expressing these channels in heterologous expression systems remains challenging. Moreover, these channels interact with multiple cellular partners *in vivo*. Thus *in vivo* studies of mutant forms of L-type calcium channels are necessary. Until now, very few of these studies have been published. Cheng et al. have described that the inactivation kinetics of the current is strongly slowed in mice carrying the Timothy syndrome mutation G406R (Cheng et al., 2011). Wu et al. have shown that skeletal muscle fibers of mice carrying the hypoPP mutation R528H exhibit an anomalous leak current through the mutated S4 segments (Wu et al., 2012). Generation of such mutant mice is still very time consuming, so developing other *in vivo* approaches could be a fruitful way to understand the effects of the multiple voltage-gated Ca^{2+} channel α_1 subunit mutations.

The nematode *Caenorhabditis elegans* Maupas could be an invaluable source for α_1 subunit mutants. Indeed, over 150 mutations have already been reported in *egl-19*, the sole gene encoding an L-type α_1 voltage-gated Ca^{2+} channel subunit in *C. elegans* (www.wormbase.org) (Lee et al., 1997). Based on their genetic and phenotypic features, *egl-19* mutants have been classified into three groups: the complete loss-of-function mutants that are lethal, the partial loss-of-function mutants that exhibit a slender morphology, and the gain-of-function mutants that are characterized by a bulky body (Lee et al., 1997). To date, the effects on currents have only been described for two partial loss-of-function mutations, *n582* and *ad1006*. The *n582* mutation changes an arginine residue to a histidine in segment IIIS4 of EGL-19. In the non-striated pharyngeal muscle cells and in the striated body wall muscle cells of *n582* mutants, voltage-dependent currents activate more slowly

CNRS, UMR 5534, Université Lyon 1, Villeurbanne, F-69622, France.

*Author for correspondence (Jospin@univ-lyon.fr)

Received 16 April 2014; Accepted 2 September 2014

The Journal of Experimental Biology (2014) doi:10.1242/jeb.106732

than those of wild-types and their voltage dependency is shifted towards positive potentials (Jospin et al., 2002; Shtonda and Avery, 2005; Gao and Zhen, 2011). In body wall muscle cells of *ad1006* mutants, voltage dependency is also shifted towards positive potentials and the current amplitude is decreased (Gao and Zhen, 2011). The functional effects of two gain-of-function mutations, *n2368* and *ad695*, have also been partially investigated: action potentials have been monitored in pharyngeal and body wall muscle cells (Lee et al., 1997; Gao and Zhen, 2011; Liu et al., 2011), and Ca^{2+} transients have been measured in the pharynx (Kerr et al., 2000). However, these studies have led to conflicting results: Gao and Zhen have shown that action potentials of *ad695* mutants are similar to those of wild-type (Gao and Zhen, 2011), whereas Liu et al. reported action potentials with longer duration and amplitude (Liu et al., 2011).

Here we describe the functional effects of *egl-19(n2368)* and *egl-19(ad695)* gain-of-function (*gf*) mutations in striated body wall muscle cells of *C. elegans*. By phenotypic and pharmacological analysis, we show that the bulky phenotype of these gain-of-function mutants is correlated with decreased locomotion, partially caused by the hypercontraction of striated body muscles. With *in situ* patch-clamp recordings we provide evidence that the hypercontraction of the muscles is due to the hyperactivation of L-type channels: the voltage dependency is shifted towards more negative potentials and the inactivation is altered. We also demonstrate that the amplitude of the voltage-dependent Ca^{2+} current is decreased in *n2368* mutants, partially due to the membrane mislocalization of the mutant channel.

RESULTS

egl-19(gf) mutants exhibit morphological and locomotion defects

As previously described (Lee et al., 1997), we found that *egl-19(ad695)* and *egl-19(n2368)* mutants were shorter than, but as wide as, wild-type animals (Fig. 1A). We quantified this size change by measuring the length and width of young adults. *egl-19(ad695)* and *egl-19(n2368)* animals were, respectively, 20 and 30% shorter than wild-type, but barely thinner (Fig. 1B). We used the width/length ratio as an indicator of body morphology (Spooner et al., 2012): a low ratio corresponds to a slender body, whereas a high ratio indicates a thickset morphology. The width/length ratios of both *egl-19(gf)* alleles are significantly higher, with *egl-19(n2368)* being greater than *egl-19(ad695)*. Both strains have a stocky body shape.

We then tested whether the stocky morphology of *egl-19(gf)* was correlated with locomotion defects. Worm locomotion was observed in liquid where animals thrash vigorously, flexing and bending their bodies. Quantification of body bends showed that this form of locomotion was reduced in both *egl-19(gf)* mutants (Fig. 1C), but more strikingly for the *n2368* strain (90% decreased). In addition, we observed that swimming of *egl-19(gf)* mutants was altered: these worms were not bending on either side like wild-type, but rather tended to curl up. We thus showed that besides morphological defects, *egl-19(gf)* worms showed quantitative and qualitative locomotion defects.

egl-19(gf) phenotype results from a high muscle tone

In their initial study, Lee et al. (Lee et al., 1997) suggested that the morphological defect of *egl-19(gf)* worms was due to a high

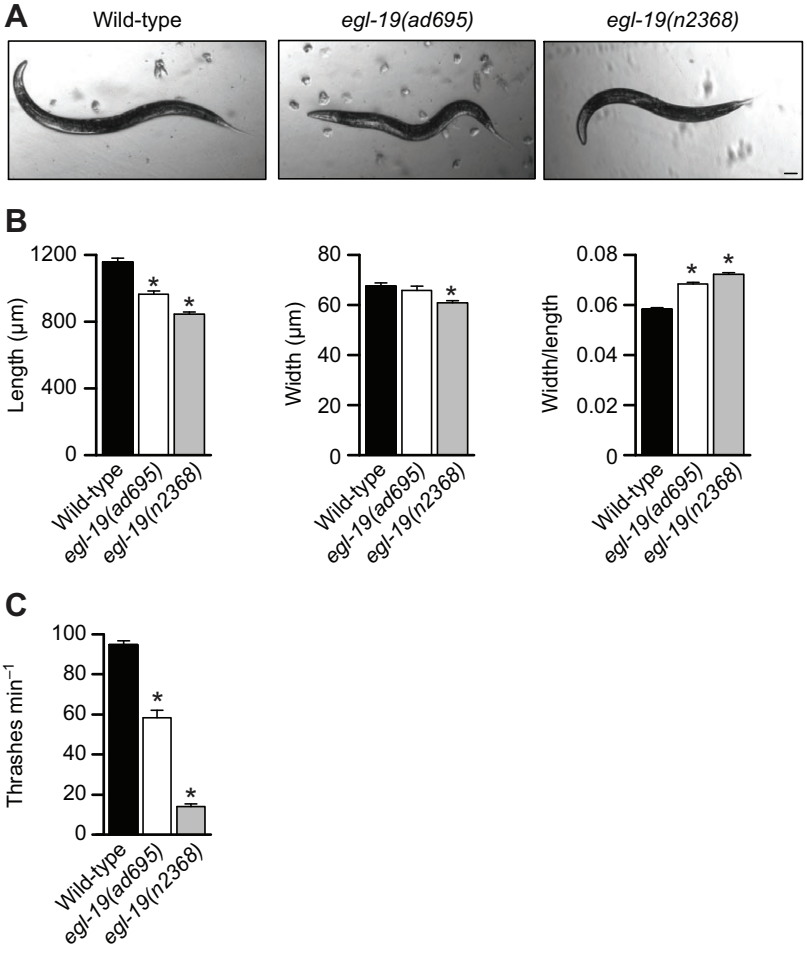

Fig. 1. *egl-19(gf)* mutants exhibit defects in body morphology and locomotion in *Caenorhabditis elegans*. (A) Representative pictures of wild-type, *egl-19(ad695)* and *egl-19(n2368)* animals. Animal heads are left, ventral sides are up. Scale bar: 100 µm. (B) Morphologic data for wild-type (*N*=31), *egl-19(ad695)* (*N*=31) and *egl-19(n2368)* (*N*=30) animals. Length was measured from the head to the region of the tail where the diameter reaches 10 µm. The length of *egl-19(gf)* mutants was significantly reduced [Kruskal–Wallis test, $P<0.0001$; Dunn's post tests: *egl-19(ad695)*/*egl-19(n2368)*, $P<0.01$; $P<0.001$ for the others]. Width was measured just behind the vulva region and was reduced in *egl-19(n2368)* worms [Kruskal–Wallis test, $P=0.002$; Dunn's post tests: wild-type/*egl-19(n2368)*, $P<0.01$; $P>0.05$ for the others]. The ratio width/length was higher in *egl-19(gf)* mutants compared with that of wild-type (ANOVA, $P<0.0001$; Bonferroni post tests: $P<0.001$ for all). Mean values ± s.e.m. are plotted. (C) Locomotion analysis of wild-type and *egl-19(gf)* mutants. Locomotion was assayed by counting the number of thrashes per minute in liquid medium at room temperature (20°C) of 20 young adults for each strain. The number was reduced in *egl-19(gf)* mutants [Kruskal–Wallis test, $P<0.0001$, Dunn's post tests: wild-type/*egl-19(ad695)*, $P<0.01$; $P<0.001$ for the others]. Mean values ± s.e.m. are plotted. Asterisks indicate a significant difference.

The Journal of Experimental Biology

The Journal of Experimental Biology (2014) doi:10.1242/jeb.106732

muscle tone. However, because *egl-19* has been shown to be involved in worm development (Tam et al., 2000; Moghal et al., 2003; Bauer Huang et al., 2007), a developmental failure could also explain the shorter size of the gain-of-function mutants. To test whether *egl-19(gf)* mutants are indeed hypercontracted, we carried out a set of pharmacological tests, adapted from Petzold et al. (Petzold et al., 2011). We took advantage of the double innervation of *C. elegans* muscles, coming from GABA and acetylcholine motor neurons, to pharmacologically induce either hypercontraction or relaxation of wild-type and *egl-19(gf)* animals. Worms were exposed to 0.1 mmol l^{-1} levamisole, a cholinergic agonist increasing muscle tone, for 30 min. As expected for a hypercontracting drug, the levamisole induced an increase of the width/length ratio for the three strains (Fig. 2A). To compare the drug responsiveness of each strain, the width/length ratio of each worm prior to treatment was subtracted from the ratio of the same worm after the 30 min treatment, and this variation was then normalized to the ratio prior to treatment, to give the levamisole-induced contraction percentage. If *egl-19(gf)* strains are already hypercontracted, they should contract less in response to levamisole. We observed that levamisole indeed affected the body morphology of wild-type animals more than that of *egl-19(gf)* mutants: after the levamisole treatment the width/length ratio varied by 24% in wild-types, whereas variations of 14 and 17% were observed in *egl-19(ad695)* and *egl-19(n2368)* mutants, respectively (Fig. 2B). Conversely, the aptitude of body wall muscles to relax was measured upon a 30 min treatment with 10 mmol l^{-1} muscimol, a GABAergic agonist inducing muscle relaxation. As expected, a decrease of the width/length ratio after muscimol treatment was observed in the three strains (Fig. 2C). The width/length ratio of each worm after the 30 min treatment was subtracted from the ratio prior to treatment of the same worm, and this variation was then normalized to the ratio prior to treatment, to give the muscimol-induced relaxation percentage. If *egl-19(gf)* worms are hypercontracted, they should relax more than wild-type animals in the presence of muscimol. Muscimol was found to have a stronger effect on *egl-19(gf)* worms compared with wild-type: after the muscimol treatment, the width/length ratio varied by 5% in wild-type, whereas variations of 7 and 11% were observed in *egl-19(ad695)* and *egl-19(n2368)* mutants, respectively (Fig. 2D). The decrease of levamisole-induced contraction and the increase of muscimol-induced relaxation in both *egl-19(gf)* mutants are in agreement with a hypercontracted basal state.

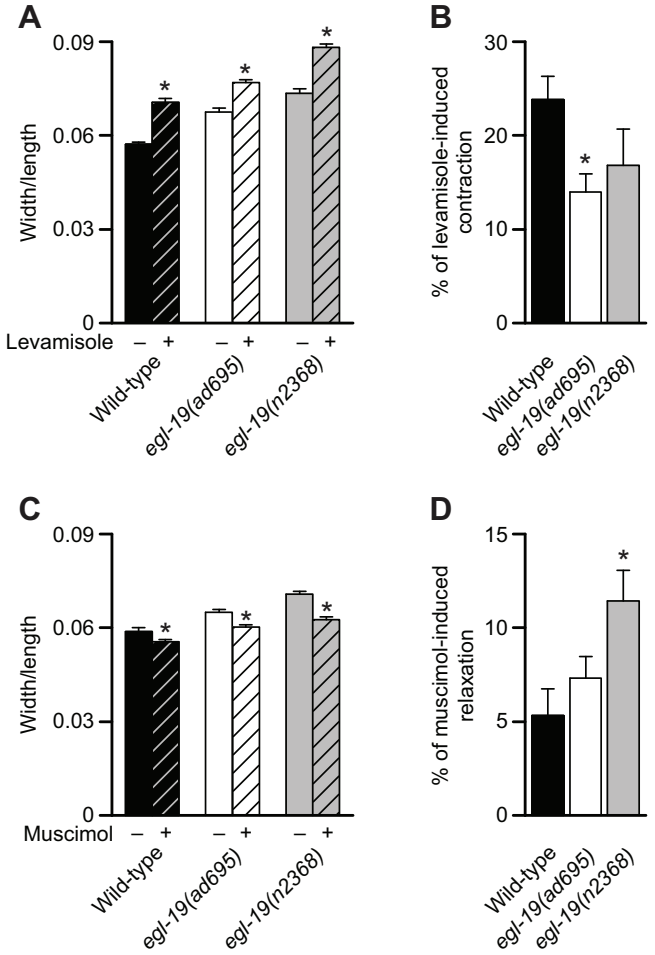

Fig. 2. *egl-19(gf)* mutants are hypercontracted. (A) Modification of the width/length ratio of wild-type and *egl-19(gf)* mutants after 30 min on 0.5 mmol l^{-1} levamisole. Ten young adults for each strain were scored. In all cases, levamisole induced an increase of the ratio, meaning an increase of body muscle tone [for wild-type and *egl-19(ad695)*, paired *t*-tests, $P<0.0001$; for *egl-19(n2368)*, Wilcoxon paired test, $P=0.0273$]. Mean values ± s.e.m. are plotted. (B) Levamisole-induced contraction percentage of wild-type and *egl-19(gf)* mutants. For each worm, the width/length prior treatment was subtracted from the ratio of the same worm after the 30 min treatment, and this variation was then normalized to the ratio prior to treatment, giving the levamisole-induced contraction percentage. The mean value ± s.e.m. was then calculated for wild-type and *egl-19(gf)* mutants ($N=10$). The levamisole-induced contraction percentage was lower in *egl-19(gf)* mutants [Kruskal–Wallis test, $P=0.0301$; Dunn's post tests: wild-type/*egl-19(ad695)*, $P<0.05$; $P>0.05$ for the others]. (C) Modification of the width/length ratio of wild-type and *egl-19(gf)* mutants after 30 min with 10 mmol l^{-1} muscimol. Ten young adults for each strain were scored. In all cases, the ratio decreased in presence of muscimol, meaning a decrease of body muscle tone [paired *t*-tests, $P=0.0073$, $P=0.0002$ and $P<0.0001$ for wild-type, *egl-19(ad695)* and *egl-19(n2368)*, respectively]. Mean values ± s.e.m. are plotted. (D) Muscimol-induced relaxation percentage of wild-type and *egl-19(gf)* mutants. For each worm, the width/length ratio after the 30 min treatment was subtracted from the ratio prior to treatment of the same worm, and this variation was then normalized to the ratio prior to treatment, giving the muscimol-induced relaxation percentage. The mean value ± s.e.m. was then calculated for wild-type and *egl-19(gf)* mutants ($N=10$). The muscimol-induced relaxation percentage was higher in *egl-19(gf)* mutants (ANOVA, $P=0.0163$; Bonferroni post test, $P<0.05$ for wild-type/*egl-19(n2368)*, $P>0.05$ for the others). Asterisks indicate a significant difference.

Voltage-gated Ca^{2+} channels are hyperactive in *egl-19(gf)* striated muscles

Using the whole-cell configuration of the patch-clamp technique in the presence of K^+ channel blockers, we investigated the properties of Ca^{2+} currents from body wall muscle cells of dissected wild-type, *egl-19(ad695)* and *egl-19(n2368)* worms. Muscle cells were depolarized by 200 ms steps from a holding potential of −60 mV. As previously described (Jospin et al., 2002), voltage-dependent Ca^{2+} currents recorded from wild-type animals displayed a biphasic appearance, with an early transient peak followed by a slowly inactivating component (Fig. 3A). This decay was altered in *egl-19(n2368)* and *egl-19(ad695)* worms: the early transient peak was difficult to distinguish in these animals (Fig. 3A,B). To confirm that inactivation was modified in *egl-19(gf)* worms, we analysed the inactivation kinetics. For each cell, we measured the R_{200} parameter, defined as the current fraction still present at the end of the pulse. We found that this fraction was significantly increased by 25 and 66% in *egl-19(ad695)* and *egl-19(n2368)* mutants, respectively, compared with that of wild-type (Fig. 3C). We also determined the activation time constant τ and showed that it is increased about 2-fold in *egl-19(n2368)* worms (Fig. 3C).

The Journal of Experimental Biology (2014) doi:10.1242/jeb.106732

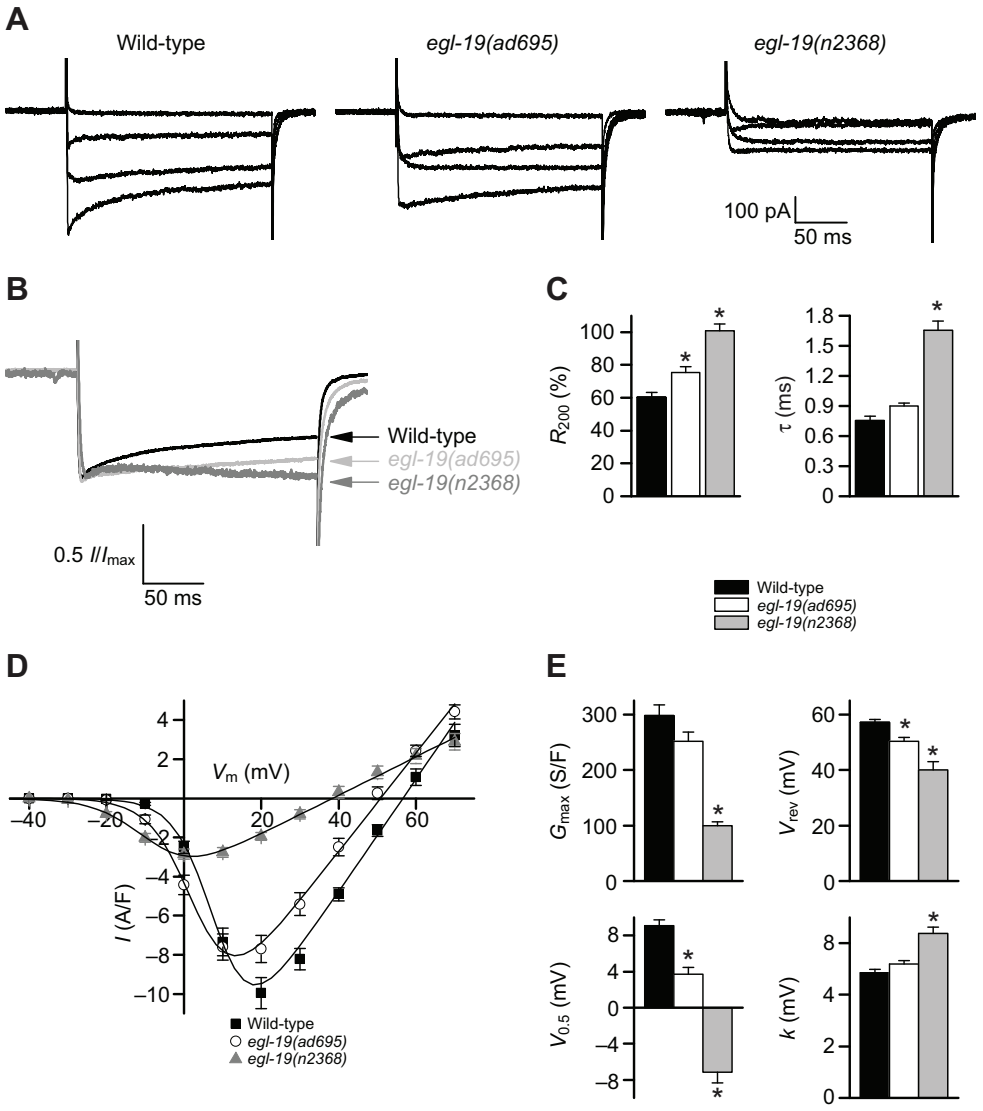

Fig. 3. Voltage-gated Ca^{2+} channels in striated muscles of *egl-19(gf)* are hyperactivated. (A) Representative traces of inward currents recorded from body muscle cells of wild-type and *egl-19(gf)* worms in response to depolarizing pulses from −60 mV to −20, 0, +20 and +40 mV. (B) Mean current traces. In each cell, the current trace of maximal amplitude, elicited by a depolarizing pulse to +20 mV for wild-type, +10 mV for *egl-19(ad695)* and 0 mV for *egl-19(n2368)*, was normalized to the peak value. Mean current traces were obtained by averaging 15 traces for wild-type, 15 traces for *egl-19(ad695)* and 12 traces for *egl-19(n2368)*. (C) Kinetics of inward currents. The fractional inactivation at the end of the pulse (R_{200}) and the time constant of activation (τ) were measured for the maximal current traces [at +20 mV for wild-type (*N*=15), +10 mV for *egl-19(ad695)* (*N*=15) and 0 mV for *egl-19(n2368)* (*N*=12)]. R_{200}, which represents the current fraction still present at the end of the pulse (Eqn 2), is higher in *egl-19(gf)* mutants compared with wild-type [ANOVA, *P*<0.0001; Bonferroni post tests: wild-type/*egl-19(ad695)*, *P*<0.05; *P*<0.001 for the others]. τ, which was obtained by fitting a single exponential function to the current from the point where the charge of capacitance was completed to the peak of the current, was higher in *egl-19(n2368)* [Kruskal–Wallis test, *P*<0.0001; Dunn's post tests: wild-type/*egl-19(ad695)*, *P*>0.05; *P*<0.001 for the others]. Mean values ± s.e.m. are plotted. (D) Mean current–voltage relationship ± s.e.m. (error bars) established at the peak of the currents from wild-type (*N*=15), *egl-19(ad695)* (*N*=15) and *egl-19(n2368)* (*N*=12) worms. Current–voltage relationships were fitted by Eqn 1. V_m, membrane potential; G_{max}, maximal conductance. (E) Ca^{2+} current parameters from body muscle cells of wild-type animals and *egl-19(gf)* animals. G_{max}, V_{rev}, $V_{0.5}$ and *k* were obtained by fitting for each cell the current–voltage relationships of the inward currents measured at the peak of the currents by Eqn 1. G_{max} was reduced only in *egl-19(n2368)* worms [Kruskal–Wallis test, *P*<0.0001; Dunn's post tests: wild-type/*egl-19(ad695)*, *P*>0.05; *P*<0.001 for the others], V_{rev} was reduced in both *egl-19(gf)* mutants [Kruskal–Wallis test, *P*<0.0001; Dunn's post tests: wild-type/*egl-19(ad695)*, *P*<0.05; wild-type/*egl-19(n2368)*, *P*<0.001; and *egl-19(ad695)*/*egl-19(n2368)*, *P*>0.05], $V_{0.5}$ was reduced in both *egl-19(gf)* mutants (ANOVA, *P*<0.0001; Bonferroni post tests, *P*<0.001 for all) and *k* was reduced only in *egl-19(n2368)* worms (ANOVA, *P*<0.0001; Bonferroni post tests: wild-type/*egl-19(ad695)*, *P*>0.05; *P*<0.001 for the others). Mean values ± s.e.m. are plotted. Asterisks indicate a significant difference.

We then established the current–voltage relationships at the maximal amplitude of the current (Fig. 3D). For each cell, individual current–voltage relationship was fitted with Eqn 1 (see Materials and methods) in order to obtain the Ca^{2+} current parameters G_{max}, V_{rev}, $V_{0.5}$ and *k* (Fig. 3E). The reversal potential V_{rev} was shifted toward negative potentials in *egl-19(ad695)* (50.2±1.4 mV) and *egl-19(n2368)* (40.0±3.0 mV) mutants, compared with that of wild-type (57.1±1.1 mV). This result suggests that voltage-gated Ca^{2+} channels might be less selective in *egl-19(gf)* animals than in wild-types. Moreover, the voltage dependency of the Ca^{2+} currents in *egl-19(gf)* mutants was altered: the half-activation potential $V_{0.5}$ was decreased by 6 and 16 mV, respectively, for *ad695* and *n2368* mutants compared with wild-type, and the steepness factor *k* was increased by 20% in *n2368* mutants. These results show that the voltage-gated

The Journal of Experimental Biology (2014) doi:10.1242/jeb.106732

Ca^{2+} channels in both *egl-19(gf)* strains are hyperactive: they open at more negative potentials because of the voltage dependency shift, and their mean open time is longer because of the partial or complete lack of the inactivation properties. Interestingly, the maximal conductance G_{max} was significantly reduced in *egl-19(n2368)* mutants, by 60% compared with the wild-type. This result could be explained by lower levels of Ca^{2+} channels at the plasma membrane, and/or by intrinsic properties of the channel, such as modification of the pore.

Voltage-gated Ca^{2+} channels are mislocalized in *egl-19(n2368)* mutants

To understand the origin of G_{max} decrease, we examined the membrane localization of voltage-gated Ca^{2+} channels in body wall muscles of wild-type, *egl-19(ad695)* and *egl-19(n2368)* worms. Because of the lack of specific antibodies, we decided to use a single-copy transgenic strain expressing a functional green fluorescent protein (GFP)-tagged voltage-gated Ca^{2+} channel to evaluate the Ca^{2+} channel localization. We generated an N-terminally GFP-tagged UNC-36 fusion protein because *unc-36* encodes the sole α_2-δ auxiliary subunit of the L-type voltage-gated Ca^{2+} channel expressed in body wall muscles (Fig. 4A) (Lainé et al., 2011) and a recent study has also shown that the interaction between α_1 and α_2-δ subunits is strong and that they are intimately associated at the plasma membrane (Cassidy et al., 2014). The expression of GFP:UNC-36 in *unc-36* mutants rescued the locomotion phenotype and the Ca^{2+} current defects observed in *unc-36* mutants (Lainé et al., 2011; Zhan et al., 2014), so we assumed that the localization of the fusion protein matched that of endogenous channels. As previously described (Frøkjaer-Jensen et al., 2006), *unc-36* staining was observed in most neuronal and muscle cells (Fig. 4B–E). The membrane fluorescence of striated muscle cells was imaged on the basal plasma membrane just above the hypodermis and showed a punctate pattern in wild-type animals (Fig. 5A). While this distribution was not affected in worms carrying the *ad695* mutation, *egl-19(n2368)* worms showed irregular dots of fewer intensity surrounded by a diffuse staining (Fig. 5A,B). In addition, the mean fluorescence was reduced by 25% in *egl-19(n2368)* animals compared with wild-type, whereas it was not affected in *egl-19(ad695)* mutants (Fig. 5C). Finally, we imaged muscles at mid-height section and observed that the fluorescence matched the diamond-shaped outline of the cells, as expected considering the plasma membrane localization of voltage-gated Ca^{2+} channels. However, we noticed an accumulation of fluorescence at the tip of the cells in *egl-19(n2368)* animals, suggesting a submembrane accumulation of these channels (Fig. 5D). These results support the

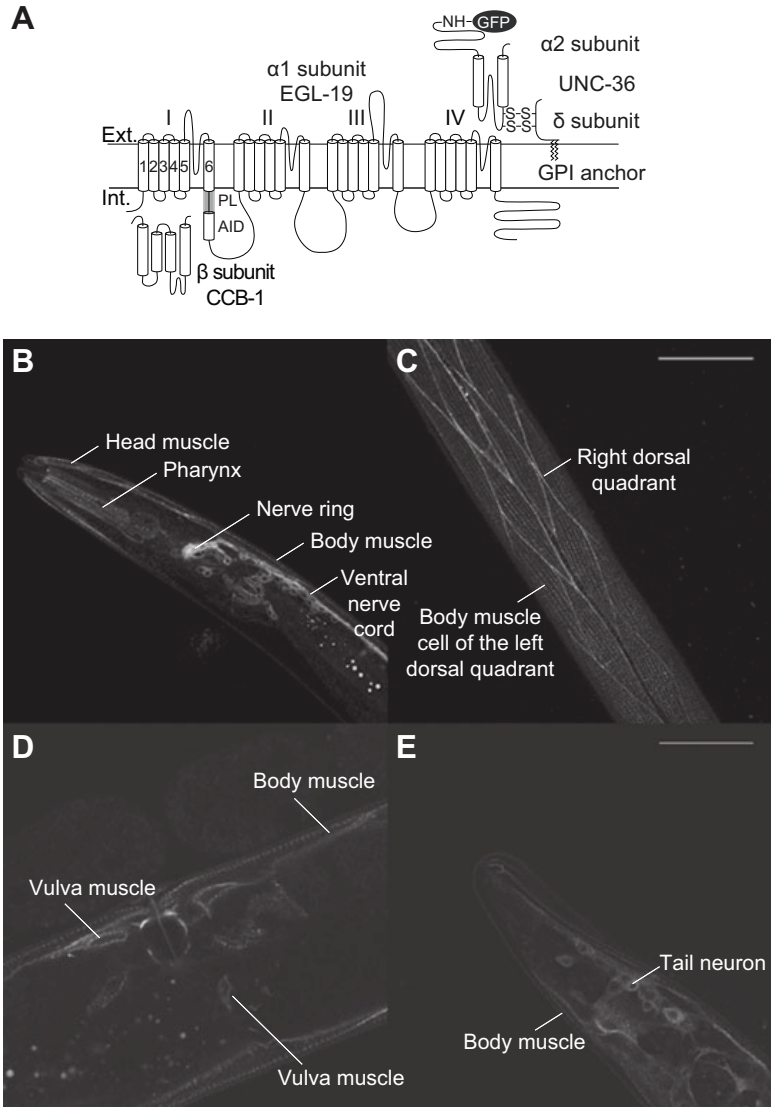

Fig. 4. The α_2-δ UNC-36 subunit is expressed in striated muscle cells among other neuronal and muscle tissues. (A) Molecular composition of the voltage-gated Ca^{2+} channels present at the plasma membrane of *C. elegans* body muscles. The main subunit α_1 EGL-19 is the voltage sensor and the pore-forming subunit, and is associated with two auxiliary subunits α2-δ and β, encoded respectively by *unc-36* and *ccb-1*. To investigate the localization of voltage-gated Ca^{2+} channels, the α_2-δ UNC-36 subunit was tagged in the N-terminus with GFP. Ext., exterior; Int., interior; PL, proximal linker; AID, alpha interaction domain; GPI, glycophosphatidylinositol. (B) Young adults expressing a *gfp::unc-36 Mos*SCI construct in an *unc-36(e251)* background were imaged on a confocal microscope with a ×63 objective (same for panels C–E). GFP fluorescence is visible in the head and body muscles, the pharynx and in most of the neurons of the head and the ventral nerve cord. Ventral side is right, head is up. (C) GFP fluorescence is detected in body muscle cells of the two dorsal quadrants. Animal is lying on the dorsal side, anterior is down. Scale bar: 50 µm for B,C. (D) GFP fluorescence is visible in body muscles, and in vulva muscles and neurons. Animal is lying on the ventral side, anterior is left. (E) GFP fluorescence is visible in body muscles and in neurons of the tail. Ventral side is left, tail is up. Scale bar: 25 µm for D,E.

The Journal of Experimental Biology (2014) doi:10.1242/jeb.106732

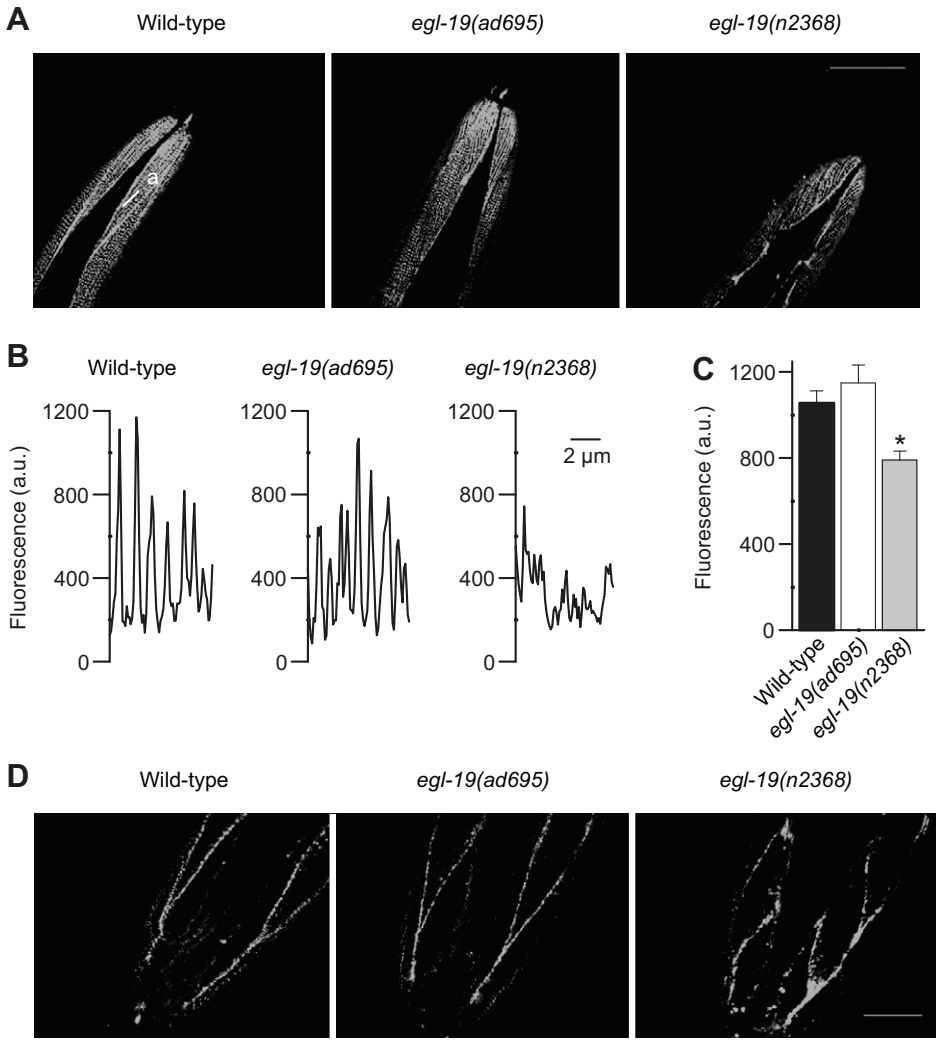

Fig. 5. Voltage-gated Ca^{2+} channels are mislocalized in *egl-19(n2368)* mutants. (A) Representative pictures of the striated muscle cells of the head from young adults expressing a *gfp::unc-36 Mos*SCI-engineered construct in wild-type, *egl-19(ad695)* and *egl-19(n2368)* backgrounds. Pictures were taken with a confocal microscope at the bottom section of muscle cells, just above the hypodermis. Heads are up. Scale bar: 25 µm. (B) Representative fluorescence profile along the fluorescent dots visible at the bottom section of head muscle cells from animals expressing a *gfp::unc-36 Mos*SCI-engineered construct in wild-type, *egl-19(ad695)* and *egl-19(n2368)* backgrounds. Fluorescence was plotted along a 7 µm line drawn in cells (a), along the axis drawn by the fluorescent dots. (C) Mean fluorescence ± s.e.m. at the basal plasma membrane of head muscle cells from animals expressing a *gfp::unc-36 Mos*SCI-engineered construct in wild-type (*N*=14), *egl-19(ad695)* (*N*=13) and *egl-19(n2368)* (*N*=13) backgrounds. For each cell, fluorescence was measured from an 18 μm^2 area in the middle region of cell (a). Mean fluorescence was reduced in *egl-19(n2368)* mutants [ANOVA, **P*=0.0009; Dunnett's post tests, *P*>0.05 for *egl-19(ad695)* and *P*<0.01 for *egl-19(n2368)*]. (D) Representative pictures of the striated muscle cells of the head from young adults expressing a *gfp::unc-36 Mos*SCI-engineered construct in wild-type, *egl-19(ad695)* and *egl-19(n2368)* backgrounds. Pictures were taken with a confocal microscope at the mid-height section of muscle cells. Fluorescence accumulates at the tip of muscle cells (asterisk) in *egl-19(n2368)* worms. Heads are down. Scale bar: 10 µm.

idea that the decrease of the maximal conductance in body wall muscles of *egl-19(n2368)* animals is at least in part due to a disrupted plasma membrane localization of the channel.

DISCUSSION

In this study, we provide a detailed characterization of two gain-of-function mutants in *egl-19*, the gene that encodes the α_1 subunit of L-type voltage-gated Ca^{2+} channels in *C. elegans* muscles. We showed that (1) the two variants *n2368* and *ad695* exhibit morphological and locomotion defects linked to a high muscle tone; (2) this high muscle tone is correlated to an increased sensitivity to the voltage of the channel and a decrease in the inactivation kinetics in both mutants; and (3) the L-type Ca^{2+} channel localization is altered in *egl-19(n2368)* mutants and the current conductance is decreased.

Why are the *egl-19(gf)* mutants hypercontracted? As in mammals, striated muscle contraction is dependent on action potentials firing (Liu et al., 2011; Liu et al., 2013); however, in *C. elegans* this firing involves voltage-gated Ca^{2+} channels and not voltage-gated Na^{+} channels (Jospin et al., 2002; Liu et al., 2011). Because of the increased sensitivity of the mutant channels to voltage, action potentials could be triggered by small depolarizations that would have no effect in wild-type. The increased propensity for action potentials would correlate with more frequent muscle contraction. Interestingly, the increase of muscle tone is more pronounced in *egl-19(n2368)* mutants, as is the modification of the voltage dependency. In *egl-19(n2368)* muscles, the shift of voltage dependency sets the current activation threshold around −30 mV instead of −20 mV in wild-type (Fig. 3D). Because the resting membrane potential of body muscle cells is typically around −25 mV in wild-type (Gao and Zhen, 2011; Liu et al., 2011) and is not different in *egl-19(n2368)* (our unpublished data), these results suggest that the voltage-gated Ca^{2+} channels are open at this potential in *egl-19(n2368)* muscles. Moreover, the slowing down of inactivation in *egl-19(n2368)* mutants might also increase the calcium flux into the cell. Thus despite the conductance decrease in this mutant, the calcium flux into the cell even at resting potential is likely to be sufficient to increase muscle tone. Alternatively, and non-exclusively, the hypercontraction could also have a neuronal origin: *egl-19* is expressed in motor neurons (Lee et al., 1997) and its partial loss-of-function specifically in these cells decreases muscle excitability (Gao and Zhen, 2011).

Muscle voltage-gated Ca^{2+} channels were visualized using a GFP-tagged α_2-δ/UNC-36 subunit and were found distributed at the boundary of body wall muscles and as a punctuated pattern at the basal membrane. This pattern is reminiscent of the one observed by Kim et al. (Kim et al., 2009) with a EGL-19-mCherry multi-copy array. These authors concluded that EGL-19 is localized near the dense bodies, which are the analogs of Z-discs coupled to the costamere adhesion complex (Lecroisey et al., 2007). Interestingly,

flattened membrane vesicles are observed around the dense bodies between the plasma membrane and the myofilaments and they have been described as sarcoplasmic reticulum cisternae (Maryon et al., 1996). Further studies will be needed to determine whether voltage-gated Ca^{2+} channels are indeed in front of the sarcoplasmic reticulum.

ad695 mutation leads an alanine-to-valine change at residue 906 in the IIIS4 segment (supplementary material Fig. S1). The S4 segments contain four to seven repeated motifs of a positive charged residue followed by two hydrophobic residues that are critical components of the voltage sensor (Noda et al., 1984; Stühmer et al., 1989; García et al., 1997). Mutations in these charged residues have been identified in L-type channels from patients suffering from hypoPP (Fontaine et al., 1994; Jurkat-Rott et al., 1994; Ptácek et al., 1994; Wang et al., 2005; Chabrier et al., 2008; Li et al., 2012). One of these mutations has been shown to allow a Ca^{2+} leak through an aberrant conduction pathway, named the gating pore or the ω pore (Wu et al., 2012). Gating pore currents have been first recorded from voltage-gated K^+ and Na^+ channels (Starace and Bezanilla, 2004; Sokolov et al., 2005; Tombola et al., 2005). Depending on the nature of the mutations, these channels are activated at resting potentials or during depolarizations, and they are permeable either to protons or to several monovalent cations. In our study we described the functional effects of the substitution of a small hydrophobic residue for a larger one. Such a mutation has never been studied before in voltage-gated Ca^{2+} channels, but the role of hydrophobic residues in S4 have been analysed in Na^+ and K^+ voltage-gated channels (Auld et al., 1990; Lopez et al., 1991; McCormack et al., 1991; Bendahhou et al., 2007; Yang et al., 2007; Elliott et al., 2012; Perry et al., 2013). Bendahhou et al. have shown for Na^+ voltage-gated channels that the size of the lateral chain can modify the half-activation potential and the inactivation kinetics (Bendahhou et al., 2007). These authors suggested that hydrophobic residues of S4 segment influence molecular interactions between S3 and S4 segments, and thus act on the voltage detection. The *ad695* mutation leads to the replacement of an alanine by another hydrophobic residue, a valine, with a bigger lateral chain; this change could thus have a similar effect on voltage sensor as the one described for Na^+ channels. Alternatively, Perry et al. have shown that mutations of the S4 hydrophobic residues in cardiac K^+ voltage-gated channels alter the inactivation kinetics by modifying the S4 and S5 interactions (Perry et al., 2013). Besides the voltage dependency and the inactivation kinetic defects, L-type Ca^{2+} currents in *egl-19(ad695)* muscles reverse at more negative potentials, indicating a decrease of Ca^{2+} selectivity. Considering the localization of *ad695* mutation in the S4 segment and the lesser selectivity for Ca^{2+} of gating pore currents, it is tempting to propose that Ca^{2+} channels in *egl-19(ad695)* muscle might support a gating pore current. Gating pore currents have never been associated with mutations other than the ones swapping arginine residues, so further studies will be needed to test this hypothesis.

The *n2368* mutation causes a substitution of glycine with arginine at residue 365 of the IS6 segment (Lee et al., 1997). This glycine residue is the second glycine of a GX_9GX_3G motif located in the lower third part of IS6, a residue conserved in all high voltage-activated calcium channels (supplementary material Fig. S1). Residue substitution experiments associated with crystal structure analysis extrapolated from K^+ channels have demonstrated that S6 segments play a central role in voltage-dependent channel gating (Zhou et al., 2001; Hohaus et al., 2005; Long et al., 2005; Zhen et al., 2005; Beyl et al., 2007; Long et al., 2007; Kudrnac et al., 2009). In particular, glycine residues of the GX_9GX_3G motif are involved in activation and inactivation mechanisms: mutations of these residues lead to a shift of the half-activation potential and a decrease of inactivation speed (Splawski et al., 2004; Splawski et al., 2005; Raybaud et al., 2006; Barrett and Tsien, 2008; Cens et al., 2008; Depil et al., 2011; Yazawa et al., 2011). Mutations of the second and third glycine have been identified in patients suffering from Timothy syndrome, a multisystem disorder mainly characterized by cardiac arrhythmias, autism and syndactyly (Splawski et al., 2004; Splawski et al., 2005). The *n2368* mutation replaces the second glycine by an arginine. Such a change has not been described before; however, the effects of replacement of this glycine by methionine, asparagine, alanine, serine or tryptophane have been analysed in rabbit L-type channels expressed in heterologous systems (Depil et al., 2011). Depending on the mutations, the half-activation potential was shifted towards more negative potentials, as we observed for *egl-19(n2368)*, or towards more positive ones. In all cases, inactivation kinetics of these mutant channels was dramatically reduced. Finally, the replacement of glycine by arginine in the *n2368* mutation creates a RX_2S motif, a consensus sequence for phosphorylation by Ca^{2+}/calmodulin-dependent protein kinase type II (CaMKII) (Kennelly and Krebs, 1991). Mutations of the third glycine have led to similar changes in some patients with Timothy syndrome. In heterologous expression systems, Erxleben et al. have shown that L-type channels carrying this kind of mutation exhibit an increase of the mean open time associated with a decrease of unitary conductance, both dependent on CaMKII activity (Erxleben et al., 2006). Thus CaMKII could also play a role in *egl-19(n2368)* mutants by modulating the properties of the mutant channels.

What is the origin of the Ca^{2+} current conductance decrease in *egl-19(n2368)* muscles? This decrease can be caused by a reduction of the channel unitary conductance, as observed by Erxleben et al. (Erxleben et al., 2006) with a similar mutation, and/or by a decrease of the channel density at the cell surface. Our data showed that the channel localization is altered in *egl-19(n2368)* mutants; so the *n2368* mutation in the IS6 segment seems at least to impair channel trafficking and/or recycling. The IS6 segment has never been shown to be involved in channel trafficking before; however, the *n2368* mutation might have an effect beyond the IS6 segment. The I–II loop downstream of IS6 is crucial for proper targeting of the channel upon β subunit binding (Pragnell et al., 1994). Structure–function studies have shown that β binding at the alpha interaction domain (AID) of I–II loop induces a coil-to-helix conformation of the proximal linker, strengthening the connection between the pore and the β subunit/I–II loop complex (Opatowsky et al., 2004; Van Petegem et al., 2004; Arias et al., 2005; Findeisen and Minor, 2009; Almagor et al., 2012). Proximal linker structure integrity is thought to be essential for β-dependent modulation of α_1 gating but its role in the localization of the channel has been less investigated (Findeisen and Minor, 2009; Gonzalez-Gutierrez et al., 2010; Almagor et al., 2012). So according to these data, the *n2368* mutation in IS6 could possibly disrupt the proximal linker integrity, decreasing β modulation of channel inactivation and α_1 trafficking. Alternatively the mislocalization of the channel may be a consequence of the mutated calcium channel hyperactivation. Ca^{2+} influx through L-type Ca^{2+} channels has been shown to couple membrane excitation to transcription (D'Arco and Dolphin, 2012). In particular, the distal C-terminal domain of L-type channels may act as a transcriptional regulator. The cleavage of this domain is thought to be Ca^{2+} dependent, and the resulting transcription factor has been shown to modulate the transcription of several genes, including the gene encoding the L-type α_1 subunit itself (Gomez-Ospina et al., 2006; Schroder et al., 2009). The increased calcium flux in *egl-19(n2368)* muscles, even at resting potentials, could

decrease *egl-19* transcription level or modify the expression of proteins involved in Ca^{2+} channel trafficking or recycling.

Now that we have characterized the effects of *egl-19(gf)* mutations on L-type voltage-dependent currents, we are planning to use these mutants to identify new partners of the L-type Ca^{2+} channel using genetic screens. In cardiomyocytes of mice, Cheng et al. have shown that downregulation of the anchoring protein AKAP150 restores normal gating of L-type Ca^{2+} channels carrying a Timothy syndrome mutation (Cheng et al., 2011). We believe that identification of new partners of this channel could lead to novel therapeutics targets for treating pathologies involving L-type channels, such as hypoPP or Timothy syndrome.

MATERIALS AND METHODS

Nematode strains and growth conditions

All *C. elegans* strains were grown at 20°C according to the method of Brenner (Brenner, 1974). N2 Bristol, DA695 *egl-19(ad695) IV*, MT6129 *egl-19(n2368) IV*, CB251 *unc-36(e251) III* and EG4322 [*ttTi5605 II, unc-119(ed9) III*] strains were provided by the *Caenorhabditis* Genetics Center (CGC, Twin Cities, MN, USA).

Molecular biology

The targeting vector (pHZ025) used to generate the *krSi3(II)* line was built as follows. A plasmid containing the *unc-36* cDNA was provided by C.I. Bargmann (Saheki and Bargmann, 2009). This plasmid was digested by *Kpn*I and *Eco*RI to remove *egfp* from the UNC-36 C-terminus, treated with T4 polymerase and circularized by self-ligation, resulting in the plasmid pHZ001. Next, *egfp* was fused in frame after the signal-peptide coding sequence in the *unc-36* cDNA by PCR fusion. First, *egfp* was amplified using oHZ07 5′-TGGCCAGCTAGCAAAGGAGAA-3′ and oHZ019 5′-TTCTTTTATGCTCTCCTTATTAAAGTCCATGCCATGTGTAATCCC-3′. Next, the *unc-36* cDNA was amplified using oHZ021 5′-ATGGCATG-GACTTTAATAAGGA-3′ and oHZ08 5′-AAAAGATCTTTTGTTTCT-TCACGATTT-3′. Both fragments were then fused by PCR fusion using oHZ07 and oHZ08 and the resulting fragment was inserted into a *Msc*I/*Bgl*II-digested pHZ001. A 2 kb region upstream of the *unc-36* open reading frame was amplified from genomic DNA using oHZ09 5′-AA-AAAAAAGCGGCCGCAAAATGCATGCAGTAATTAGTGTCC-3′ and oHZ010 5′-TGGCCACTTATTAAAACTGCTTGT-3′, and this sequence was inserted into the previous plasmid after *Not*I and *Msc*I digestion, resulting in plasmid pHZ009. Finally, the transgene sequence (*Punc-36::egfp::unc-36::3′UTR unc-54*) was released from pHZ009 using *Not*I and *Apa*I, blunted using T4 polymerase and inserted into the pCFJ151 vector backbone, resulting in pHZ025.

We followed the direct-insertion *Mos*SCI protocol (Frøkjaer-Jensen et al., 2008) to generate *krSi3*. In brief, we micro-injected the gonads of EG4322 worms with a DNA mix containing: the targeting vector pHZ025 at 50 ng µl^{-1}, pJL43.1 at 50 ng µl^{-1} (*Mos* transposases expressed under germline constitutive promoter P*glh-2*), and transformation markers *Pmyo3::gfp* at 10 ng µl^{-1} and *Prab3::gfp* at 10 ng µl^{-1}. *Mos*SCI events were selected by screening for the restoration of wild-type locomotion and loss of the transformation markers. The *krSi3* insertion was validated by PCR using oCF418 5′-TCTGGCTCTGCTTCTTCGTT-3′ and oCF419 5′-CAAT-TCATCCCGGTTTCTGT-3′ (Frøkjaer-Jensen et al., 2008). *krSi3* was subsequently crossed into the *unc-36(e251)* null mutant, resulting in EN5403 *krSi3*[*Punc-36::egfp::unc-36, cb-unc-119* (+)] *II; unc-36(e251) III*. EN5403 was further crossed with *egl-19(ad695)* and *egl-19(n2368)* to generate KAG200 and KAG214, respectively. All enzymes were obtained from Thermo Fisher Scientific (Waltham, MA, USA).

Phenotype analysis and pharmacology

For morphological analysis, 20–30 L4 larvae were placed on freshly seeded nematode growth medium (NGM) plates at 15°C. The following day, individual worms were transferred into a small drop of M9 buffer and imaged on an Olympus IMT2 (Hamburg, Germany) microscope. The animal width and length were determined using ImageJ software (NIH Image, Bethesda, MD, USA): length was measured using a segmented-line spline fit from the tip of the nose to the region where the tail is 10 µm wide, and width was measured just posterior to the vulva. In pharmacological assays, 10 young adult worms were imaged after a 30 min incubation with 0.5 mmol l^{-1} levamisole or 10 mmol l^{-1} muscimol. For each animal the ratio width/length was determined before and after the drug treatment and the percentage of variation was calculated.

For locomotion tests, 10–20 L4 larvae were placed on freshly seeded NGM plates at 15°C. The following day, individual animals were transferred into a microtiter well (Corning Inc., Corning, NY, USA) containing 50 µl of M9 buffer on top of 2% agar in M9. After a 2 min recovery period, thrashes were counted for 1 min. A thrash was defined by Miller et al. (Miller et al., 1996) as a change in the direction of bending at the mid-body. All chemical were obtained from Sigma-Aldrich (St Louis, MO, USA).

Electrophysiology

Microdissection of *C. elegans* and electrophysiological methods were performed as described previously by Lainé et al. (Lainé et al., 2011). Membrane currents were recorded in the whole-cell configuration using an RK-400 patch-clamp amplifier (Bio-Logic, Claix, France). Acquisition and command voltage were controlled using pCLAMP9 software driving a 1322A Digidata (Molecular Devices, Sunnyvale, CA, USA). Data were analysed and graphed using pCLAMP9 and Origin (OriginLab, Northampton, MA, USA) software. The resistance of recording pipettes ranged between 2.5 and 3 MΩ. Recordings were performed after 1 min dialysis only on cells exhibiting resistances above 800 MΩ. Capacitance and resistance were not compensated.

For whole-cell Ca^{2+} currents, the bath solution contained (mmol l^{-1}): 140 tetraethylammonium chloride (TEACl), 6 $CaCl_2$, 5 $MgCl_2$, 3 4-aminopyridine (4-AP), 10 Hepes and sucrose to 337 mosmol l^{-1} (pH 7.2); and the pipette solution contained (mmol l^{-1}): 140 CsCl, 5 TEACl, 5 EGTA, 5 Hepes, 4 MgATP and sucrose to 328 mosmol l^{-1} (pH 7.2). The membrane potential was held at −60 mV, and currents were recorded by applying 200 ms voltage steps from −70 to +70 mV in 10 mV increments. Leak currents were subtracted from all recordings. Current–voltage relationships were established by measuring the currents at the peak of the current and were fitted with the following equation:

$$I(v) = \frac{G_{\max}(v - V_{\text{rev}})}{1 + e^{[(V_{0.5} - v)/k]}}, \quad (1)$$

where $I(v)$ is the measured density of current, v is the test voltage pulse, $G_{\max}$ is the maximum conductance, V_{rev} is the reversal potential, $V_{0.5}$ is the half-activation voltage and k is the steepness factor. To plot the mean current traces, the current trace of maximal amplitude was normalized to the peak current intensity for each cell, and then averaged. The time constant of activation (τ) was obtained by fitting a single exponential function to the current from the point where the charge of capacitance was completed to the peak of the current. The fractional inactivation R_{200} represents the current fraction still present at the end of the pulse:

$$R_{200} = \frac{I_{200\text{ms}}}{I_{\text{peak}}}. \quad (2)$$

All experiments were done at room temperature.

Fluorescence microscopy

Young adults carrying *krSi3* were transferred into a drop of M9 containing 20 mmol l^{-1} sodium azide on a top of an agarose pad. Animals were imaged on an inverted LSM 5 Exciter laser scanning confocal microscope (Zeiss, Oberkochen, Germany) equipped with a ×63 oil immersion objective, ×1.4 numerical aperture. GFP was excited at 488 nm, and the emission from 505 to 600 nm was collected. Muscle cells were imaged in the head region of the animals and were analysed with the software ImageJ (NIH Image, Bethesda, MD, USA). Mean fluorescence of basal plasma membrane was quantified from an 18 µm^2 area in the middle region of the cells.

Acknowledgements

We thank the *Caenorhabditis* Genetics Center, which is funded by the National Institutes of Health (NIH) Office of Research Infrastructure Programs (P40 OD010440) for strains, C. I. Bargmann for cDNA, M. Peters and T. Boulin for

critical reading of the manuscript, and K. Gieseler and B. Allard for sharing facilities and scientific inputs.

Competing interests
The authors declare no competing financial interests.

Author contributions
V.L. designed, performed and analysed the experiments and wrote the manuscript. J.R.S. performed and analysed the experiments. H.Z. performed and analysed the experiments. J.-L.B. wrote the manuscript. M.J. designed, performed and analysed the experiments and wrote the manuscript.

Funding
This work was supported by the Centre National de la Recherche Scientifique, the Université Lyon 1, the Société Française de Myologie, the Fondation Pierre Gilles de Gennes and the Fédération pour la Recherche Médicale.

Supplementary material
Supplementary material available online at
http://jeb.biologists.org/lookup/suppl/doi:10.1242/jeb.106732/-/DC1

References
Almagor, L., Chomsky-Hecht, O., Ben-Mocha, A., Hendin-Barak, D., Dascal, N. and Hirsch, J. A. (2012). The role of a voltage-dependent Ca^{2+} channel intracellular linker: a structure−function analysis. *J. Neurosci.* **32**, 7602-7613.

Arias, J. M., Murbartián, J., Vitko, I., Lee, J.-H. and Perez-Reyes, E. (2005). Transfer of β subunit regulation from high to low voltage-gated Ca^{2+} channels. *FEBS Lett.* **579**, 3907-3912.

Auld, V. J., Goldin, A. L., Krafte, D. S., Catterall, W. A., Lester, H. A., Davidson, N. and Dunn, R. J. (1990). A neutral amino acid change in segment IIS4 dramatically alters the gating properties of the voltage-dependent sodium channel. *Proc. Natl. Acad. Sci. USA* **87**, 323-327.

Barrett, C. F. and Tsien, R. W. (2008). The Timothy syndrome mutation differentially affects voltage- and calcium-dependent inactivation of CaV1.2 L-type calcium channels. *Proc. Natl. Acad. Sci. USA* **105**, 2157-2162.

Bauer Huang, S. L., Saheki, Y., VanHoven, M. K., Torayama, I., Ishihara, T., Katsura, I., van der Linden, A., Sengupta, P. and Bargmann, C. I. (2007). Left-right olfactory asymmetry results from antagonistic functions of voltage-activated calcium channels and the Raw repeat protein OLRN-1 in *C. elegans*. *Neural Dev.* **2**, 24.

Bendahhou, S., O'Reilly, A. O. and Duclohier, H. (2007). Role of hydrophobic residues in the voltage sensors of the voltage-gated sodium channel. *Biochim. Biophys. Acta* **1768**, 1440-1447.

Beyl, S., Timin, E. N., Hohaus, A., Stary, A., Kudrnac, M., Guy, R. H. and Hering, S. (2007). Probing the architecture of an L-type calcium channel with a charged phenylalkylamine: evidence for a widely open pore and drug trapping. *J. Biol. Chem.* **282**, 3864-3870.

Brenner, S. (1974). The genetics of *Caenorhabditis elegans*. *Genetics* **77**, 71-94.

Carpenter, D., Ringrose, C., Leo, V., Morris, A., Robinson, R. L., Halsall, P. J., Hopkins, P. M. and Shaw, M.-A. (2009). The role of CACNA1S in predisposition to malignant hyperthermia. *BMC Med. Genet.* **10**, 104.

Cassidy, J. S., Ferron, L., Kadurin, I., Pratt, W. S. and Dolphin, A. C. (2014). Functional exofacially tagged N-type calcium channels elucidate the interaction with auxiliary $\alpha_2\delta$-1 subunits. *Proc. Natl. Acad. Sci. USA* **111**, 8979-8984.

Catterall, W. A. (2011). Voltage-gated calcium channels. *Cold Spring Harb. Perspect. Biol.* **3**, a003947.

Cens, T., Leyris, J.-P. and Charnet, P. (2008). Introduction into Ca(v)2.1 of the homologous mutation of Ca(v)1.2 causing the Timothy syndrome questions the role of V421 in the phenotypic definition of P-type Ca^{2+} channel. *Pflugers Arch.* **457**, 417-430.

Chabrier, S., Monnier, N. and Lunardi, J. (2008). Early onset of hypokalaemic periodic paralysis caused by a novel mutation of the CACNA1S gene. *J. Med. Genet.* **45**, 686-688.

Cheng, E. P., Yuan, C., Navedo, M. F., Dixon, R. E., Nieves-Cintrón, M., Scott, J. D. and Santana, L. F. (2011). Restoration of normal L-type Ca^{2+} channel function during Timothy syndrome by ablation of an anchoring protein. *Circ. Res.* **109**, 255-261.

D'Arco, M. and Dolphin, A. C. (2012). L-type calcium channels: on the fast track to nuclear signaling. *Sci. Signal.* **5**, pe34.

Depil, K., Beyl, S., Stary-Weinzinger, A., Hohaus, A., Timin, E. and Hering, S. (2011). Timothy mutation disrupts the link between activation and inactivation in Ca(V)1.2 protein. *J. Biol. Chem.* **286**, 31557-31564.

Elliott, D. J. S., Neale, E. J., Munsey, T. S., Bannister, J. P. and Sivaprasadarao, A. (2012). Role of hydrophobic and ionic forces in the movement of S4 of the Shaker potassium channel. *Mol. Membr. Biol.* **29**, 321-332.

Erxleben, C., Liao, Y., Gentile, S., Chin, D., Gomez-Alegria, C., Mori, Y., Birnbaumer, L. and Armstrong, D. L. (2006). Cyclosporin and Timothy syndrome increase mode 2 gating of CaV1.2 calcium channels through aberrant phosphorylation of S6 helices. *Proc. Natl. Acad. Sci. USA* **103**, 3932-3937.

Findeisen, F. and Minor, D. L., Jr (2009). Disruption of the IS6-AID linker affects voltage-gated calcium channel inactivation and facilitation. *J. Gen. Physiol.* **133**, 327-343.

Fontaine, B., Vale-Santos, J., Jurkat-Rott, K., Reboul, J., Plassart, E., Rime, C. S., Elbaz, A., Heine, R., Guimarães, J., Weissenbach, J. et al. (1994). Mapping of the hypokalaemic periodic paralysis (HypoPP) locus to chromosome 1q31-32 in three European families. *Nat. Genet.* **6**, 267-272.

Frøkjaer-Jensen, C., Kindt, K. S., Kerr, R. A., Suzuki, H., Melnik-Martinez, K., Gerstbreih, B., Driscol, M. and Schafer, W. R. (2006). Effects of voltage-gated calcium channel subunit genes on calcium influx in cultured *C. elegans* mechanosensory neurons. *J. Neurobiol.* **66**, 1125-1139.

Frøkjaer-Jensen, C., Davis, M. W., Hopkins, C. E., Newman, B. J., Thummel, J. M., Olesen, S.-P., Grunnet, M. and Jorgensen, E. M. (2008). Single-copy insertion of transgenes in *Caenorhabditis elegans*. *Nat. Genet.* **40**, 1375-1383.

Gao, S. and Zhen, M. (2011). Action potentials drive body wall muscle contractions in *Caenorhabditis elegans*. *Proc. Natl. Acad. Sci. USA* **108**, 2557-2562.

García, J., Nakai, J., Imoto, K. and Beam, K. G. (1997). Role of S4 segments and the leucine heptad motif in the activation of an L-type calcium channel. *Biophys. J.* **72**, 2515-2523.

Gomez-Ospina, N., Tsuruta, F., Barreto-Chang, O., Hu, L. and Dolmetsch, R. (2006). The C terminus of the L-type voltage-gated calcium channel Ca(V)1.2 encodes a transcription factor. *Cell* **127**, 591-606.

Gonzalez-Gutierrez, G., Miranda-Laferte, E., Contreras, G., Neely, A. and Hidalgo, P. (2010). Swapping the I−II intracellular linker between L-type CaV1.2 and R-type CaV2.3 high-voltage gated calcium channels exchanges activation attributes. *Channels* **4**, 42-50.

Hirano, M., Kokunai, Y., Nagai, A., Nakamura, Y., Saigoh, K., Kusunoki, S. and Takahashi, M. P. (2011). A novel mutation in the calcium channel gene in a family with hypokalemic periodic paralysis. *J. Neurol. Sci.* **309**, 9-11.

Hohaus, A., Beyl, S., Kudrnac, M., Berjukow, S., Timin, E. N., Marksteiner, R., Maw, M. A. and Hering, S. (2005). Structural determinants of L-type channel activation in segment IIS6 revealed by a retinal disorder. *J. Biol. Chem.* **280**, 38471-38477.

Jospin, M., Jacquemond, V., Mariol, M.-C., Ségalat, L. and Allard, B. (2002). The L-type voltage-dependent Ca^{2+} channel EGL-19 controls body wall muscle function in *Caenorhabditis elegans*. *J. Cell Biol.* **159**, 337-348.

Jurkat-Rott, K., Lehmann-Horn, F., Elbaz, A., Heine, R., Gregg, R. G., Hogan, K., Powers, P. A., Lapie, P., Vale-Santos, J. E., Weissenbach, J. et al. (1994). A calcium channel mutation causing hypokalemic periodic paralysis. *Hum. Mol. Genet.* **3**, 1415-1419.

Ke, T., Gomez, C. R., Mateus, H. E., Castano, J. A. and Wang, Q. K. (2009). Novel CACNA1S mutation causes autosomal dominant hypokalemic periodic paralysis in a South American family. *J. Hum. Genet.* **54**, 660-664.

Kennelly, P. J. and Krebs, E. G. (1991). Consensus sequences as substrate specificity determinants for protein kinases and protein phosphatases. *J. Biol. Chem.* **266**, 15555-15558.

Kerr, R., Lev-Ram, V., Baird, G., Vincent, P., Tsien, R. Y. and Schafer, W. R. (2000). Optical imaging of calcium transients in neurons and pharyngeal muscle of *C. elegans*. *Neuron* **26**, 583-594.

Kim, H., Pierce-Shimomura, J. T., Oh, H. J., Johnson, B. E., Goodman, M. B. and McIntire, S. L. (2009). The dystrophin complex controls BK channel localization and muscle activity in *Caenorhabditis elegans*. *PLoS Genet.* **5**, e1000780.

Kudrnac, M., Beyl, S., Hohaus, A., Stary, A., Peterbauer, T., Timin, E. and Hering, S. (2009). Coupled and independent contributions of residues in IS6 and IIS6 to activation gating of CaV1.2. *J. Biol. Chem.* **284**, 12276-12284.

Lainé, V., Frøkjær-Jensen, C., Couchoux, H. and Jospin, M. (2011). The α1 subunit EGL-19, the α2/δ subunit UNC-36, and the β subunit CCB-1 underlie voltage-dependent calcium currents in *Caenorhabditis elegans* striated muscle. *J. Biol. Chem.* **286**, 36180-36187.

Lecroisey, C., Ségalat, L. and Gieseler, K. (2007). The *C. elegans* dense body: anchoring and signaling structure of the muscle. *J. Muscle Res. Cell Motil.* **28**, 79-87.

Lee, R. Y., Lobel, L., Hengartner, M., Horvitz, H. R. and Avery, L. (1997). Mutations in the α1 subunit of an L-type voltage-activated Ca^{2+} channel cause myotonia in *Caenorhabditis elegans*. *EMBO J.* **16**, 6066-6076.

Li, F.-F., Li, Q.-Q., Tan, Z.-X., Zhang, S.-Y., Liu, J., Zhao, E. Y., Yu, G.-C., Zhou, J., Zhang, L.-M. and Liu, S.-L. (2012). A novel mutation in CACNA1S gene associated with hypokalemic periodic paralysis which has a gender difference in the penetrance. *J. Mol. Neurosci.* **46**, 378-383.

Liu, P., Ge, Q., Chen, B., Salkoff, L., Kotlikoff, M. I. and Wang, Z.-W. (2011). Genetic dissection of ion currents underlying all-or-none action potentials in *C. elegans* body-wall muscle cells. *J. Physiol.* **589**, 101-117.

Liu, P., Chen, B. and Wang, Z.-W. (2013). Postsynaptic current bursts instruct action potential firing at a graded synapse. *Nat. Commun.* **4**, 1911.

Long, S. B., Campbell, E. B. and Mackinnon, R. (2005). Crystal structure of a mammalian voltage-dependent Shaker family K^+ channel. *Science* **309**, 897-903.

Long, S. B., Tao, X., Campbell, E. B. and MacKinnon, R. (2007). Atomic structure of a voltage-dependent K^+ channel in a lipid membrane-like environment. *Nature* **450**, 376-382.

Lopez, G. A., Jan, Y. N. and Jan, L. Y. (1991). Hydrophobic substitution mutations in the S4 sequence alter voltage-dependent gating in Shaker K^+ channels. *Neuron* **7**, 327-336.

Maryon, E. B., Coronado, R. and Anderson, P. (1996). unc-68 encodes a ryanodine receptor involved in regulating *C. elegans* body-wall muscle contraction. *J. Cell Biol.* **134**, 885-893.

McCormack, K., Tanouye, M. A., Iverson, L. E., Lin, J. W., Ramaswami, M., McCormack, T., Campanelli, J. T., Mathew, M. K. and Rudy, B. (1991). A role for hydrophobic residues in the voltage-dependent gating of Shaker K^+ channels. *Proc. Natl. Acad. Sci. USA* **88**, 2931-2935.

Miller, K. G., Alfonso, A., Nguyen, M., Crowell, J. A., Johnson, C. D. and Rand, J. B. (1996). A genetic selection for *Caenorhabditis elegans* synaptic transmission mutants. *Proc. Natl. Acad. Sci. USA* **93**, 12593-12598.

Moghal, N., Garcia, L. R., Khan, L. A., Iwasaki, K. and Sternberg, P. W. (2003). Modulation of EGF receptor-mediated vulva development by the heterotrimeric G-protein Gαq and excitable cells in *C. elegans*. *Development* **130**, 4553-4566.

Monnier, N., Procaccio, V., Stieglitz, P. and Lunardi, J. (1997). Malignant-hyperthermia susceptibility is associated with a mutation of the α1-subunit of the human dihydropyridine-sensitive L-type voltage-dependent calcium-channel receptor in skeletal muscle. *Am. J. Hum. Genet.* **60**, 1316-1325.

Noda, M., Shimizu, S., Tanabe, T., Takai, T., Kayano, T., Ikeda, T., Takahashi, H., Nakayama, H., Kanaoka, Y., Minamino, N. et al. (1984). Primary structure of *Electrophorus electricus* sodium channel deduced from cDNA sequence. *Nature* **312**, 121-127.

Opatowsky, Y., Chen, C.-C., Campbell, K. P. and Hirsch, J. A. (2004). Structural analysis of the voltage-dependent calcium channel β subunit functional core and its complex with the α1 interaction domain. *Neuron* **42**, 387-399.

Perry, M. D., Wong, S., Ng, C. A. and Vandenberg, J. I. (2013). Hydrophobic interactions between the voltage sensor and pore mediate inactivation in Kv11.1 channels. *J. Gen. Physiol.* **142**, 275-288.

Petzold, B. C., Park, S.-J., Ponce, P., Roozeboom, C., Powell, C., Goodman, M. B. and Pruitt, B. L. (2011). *Caenorhabditis elegans* body mechanics are regulated by body wall muscle tone. *Biophys. J.* **100**, 1977-1985.

Pirone, A., Schredelseker, J., Tuluc, P., Gravino, E., Fortunato, G., Flucher, B. E., Carsana, A., Salvatore, F. and Grabner, M. (2010). Identification and functional characterization of malignant hyperthermia mutation T1354S in the outer pore of the Cavα1S-subunit. *Am. J. Physiol.* **299**, C1345-C1354.

Pragnell, M., De Waard, M., Mori, Y., Tanabe, T., Snutch, T. P. and Campbell, K. P. (1994). Calcium channel β-subunit binds to a conserved motif in the I–II cytoplasmic linker of the α 1-subunit. *Nature* **368**, 67-70.

Ptácek, L. J., Tawil, R., Griggs, R. C., Engel, A. G., Layzer, R. B., Kwieciński, H., McManis, P. G., Santiago, L., Moore, M., Fouad, G. et al. (1994). Dihydropyridine receptor mutations cause hypokalemic periodic paralysis. *Cell* **77**, 863-868.

Raybaud, A., Dodier, Y., Bissonnette, P., Simoes, M., Bichet, D. G., Sauvé, R. and Parent, L. (2006). The role of the GX9GX3G motif in the gating of high voltage-activated Ca^{2+} channels. *J. Biol. Chem.* **281**, 39424-39436.

Saheki, Y. and Bargmann, C. I. (2009). Presynaptic CaV2 calcium channel traffic requires CALF-1 and the α(2)δ subunit UNC-36. *Nat. Neurosci.* **12**, 1257-1265.

Schroder, E., Byse, M. and Satin, J. (2009). L-type calcium channel C-terminus autoregulates transcription. *Circ. Res.* **104**, 1373-1381.

Shtonda, B. and Avery, L. (2005). CCA-1, EGL-19 and EXP-2 currents shape action potentials in the *Caenorhabditis elegans* pharynx. *J. Exp. Biol.* **208**, 2177-2190.

Sokolov, S., Scheuer, T. and Catterall, W. A. (2005). Ion permeation through a voltage-sensitive gating pore in brain sodium channels having voltage sensor mutations. *Neuron* **47**, 183-189.

Splawski, I., Timothy, K. W., Sharpe, L. M., Decher, N., Kumar, P., Bloise, R., Napolitano, C., Schwartz, P. J., Joseph, R. M., Condouris, K. et al. (2004). Ca(V)1.2 calcium channel dysfunction causes a multisystem disorder including arrhythmia and autism. *Cell* **119**, 19-31.

Splawski, I., Timothy, K. W., Decher, N., Kumar, P., Sachse, F. B., Beggs, A. H., Sanguinetti, M. C. and Keating, M. T. (2005). Severe arrhythmia disorder caused by cardiac L-type calcium channel mutations. *Proc. Natl. Acad. Sci. USA* **102**, 8089-8096, discussion 8086-8088.

Spooner, P. M., Bonner, J., Maricq, A. V., Benian, G. M. and Norman, K. R. (2012). Large isoforms of UNC-89 (obscurin) are required for muscle cell architecture and optimal calcium release in *Caenorhabditis elegans*. *PLoS ONE* **7**, e40182.

Starace, D. M. and Bezanilla, F. (2004). A proton pore in a potassium channel voltage sensor reveals a focused electric field. *Nature* **427**, 548-553.

Stühmer, W., Conti, F., Suzuki, H., Wang, X. D., Noda, M., Yahagi, N., Kubo, H. and Numa, S. (1989). Structural parts involved in activation and inactivation of the sodium channel. *Nature* **339**, 597-603.

Tam, T., Mathews, E., Snutch, T. P. and Schafer, W. R. (2000). Voltage-gated calcium channels direct neuronal migration in *Caenorhabditis elegans*. *Dev. Biol.* **226**, 104-117.

Tombola, F., Pathak, M. M. and Isacoff, E. Y. (2005). Voltage-sensing arginines in a potassium channel permeate and occlude cation-selective pores. *Neuron* **45**, 379-388.

Toppin, P. J., Chandy, T. T., Ghanekar, A., Kraeva, N., Beattie, W. S. and Riazi, S. (2010). A report of fulminant malignant hyperthermia in a patient with a novel mutation of the CACNA1S gene. *Can. J. Anaesth.* **57**, 689-693.

Van Petegem, F., Clark, K. A., Chatelain, F. C. and Minor, D. L., Jr (2004). Structure of a complex between a voltage-gated calcium channel β-subunit and an α-subunit domain. *Nature* **429**, 671-675.

Wang, Q., Liu, M., Xu, C., Tang, Z., Liao, Y., Du, R., Li, W., Wu, X., Wang, X., Liu, P. et al. (2005). Novel CACNA1S mutation causes autosomal dominant hypokalemic periodic paralysis in a Chinese family. *J. Mol. Med.* **83**, 203-208.

Wu, F., Mi, W., Hernández-Ochoa, E. O., Burns, D. K., Fu, Y., Gray, H. F., Struyk, A. F., Schneider, M. F. and Cannon, S. C. (2012). A calcium channel mutant mouse model of hypokalemic periodic paralysis. *J. Clin. Invest.* **122**, 4580-4591.

Yang, Y.-C., Own, C.-J. and Kuo, C.-C. (2007). A hydrophobic element secures S4 voltage sensor in position in resting Shaker K^+ channels. *J. Physiol.* **582**, 1059-1072.

Yazawa, M., Hsueh, B., Jia, X., Pasca, A. M., Bernstein, J. A., Hallmayer, J. and Dolmetsch, R. E. (2011). Using induced pluripotent stem cells to investigate cardiac phenotypes in Timothy syndrome. *Nature* **471**, 230-234.

Zhan, H., Stanciauskas, R., Stigloher, C., Dizon, K. K., Jospin, M., Bessereau, J. L. and Pinaud, F. (2014). *In vivo* single-molecule imaging identifies altered dynamics of calcium channels in dystrophin-mutant *C. elegans*. *Nature Comm.* (in press).

Zhen, X.-G., Xie, C., Fitzmaurice, A., Schoonover, C. E., Orenstein, E. T. and Yang, J. (2005). Functional architecture of the inner pore of a voltage-gated Ca^{2+} channel. *J. Gen. Physiol.* **126**, 193-204.

Zhou, Y., Morais-Cabral, J. H., Kaufman, A. and MacKinnon, R. (2001). Chemistry of ion coordination and hydration revealed by a K^+ channel-Fab complex at 2.0 A resolution. *Nature* **414**, 43-48.